ELSEVIER

Contents lists available at ScienceDirect

# Thermochimica Acta

journal homepage: www.elsevier.com/locate/tca





# Crystallization kinetics of glass fiber filled poly(ether ether ketone) with nanogram sample size: Feasibility study for fast scanning calorimetry

Xiaoshi Zhang <sup>a, 1</sup>, Jason D. Alexander <sup>b, 1</sup>, Jiho Seo <sup>b</sup>, Anne M. Gohn <sup>a</sup>, Matthew J. Behary <sup>a</sup>, Richard P. Schaake <sup>c</sup>, Ralph H. Colby <sup>b</sup>, Alicyn M. Rhoades <sup>a, \*</sup>

- <sup>a</sup> Plastics Engineering Technology, Penn State Behrend, Erie, Pennsylvania, USA
- <sup>b</sup> Department of Materials Science and Engineering, Penn State University, University Park, Pennsylvania, USA
- <sup>c</sup> Materials & Materials Processing, SKF Research & Technology Development, Houten, the Netherlands

#### ARTICLE INFO

# Keywords: Poly(ether ether ketone) Composites Crystallization kinetics X-ray computed tomography Fast scanning calorimetry

#### ABSTRACT

The feasibility of using FSC for fiber-filled polymer composites is questionable since the typical FSC sample thickness is comparable to the fiber diameter. In this study, X-ray computed tomography (XCT) with an ultrahigh-resolution was performed to reconstruct the interior structure of poly(ether ether) ketone (PEEK) composite pellets. Using reconstructed 3D XCT matrices of PEEK resin, glass fibers, and voids, PEEK pellets sliced with different directions and sampling frequencies were analyzed to mimic FSC sample preparation. For the sample thicknesses less than  $50~\mu m$ , PEEK samples sliced perpendicular to the fiber flow direction had good filler homogeneity and always had a lower coefficient of variation than pellets sliced along the fiber flow direction. This conclusion is later supported by the isothermal crystallization kinetics of PEEK and its composites investigated by differential scanning calorimetry and fast scanning calorimetry over a wide temperature range relevant to processing.

#### 1. Introduction

Poly(ether ether ketone) (PEEK) is a high-performance thermoplastic with many promising properties. Due to its rigid aromatic structures in the repeating unit, PEEK has a higher glass transition temperature, melting temperature, and degradation temperature compared to most commodity plastics and engineering plastics [1]. Besides that, PEEK is well-known for its excellent modulus, toughness, and chemical and wear resistance [2]. These superior properties allow PEEK to be used in advanced engineering applications that require long-term reliable performance, including aerospace, electrical & electronics, automotive, defense, medical, etc. Incorporating other materials, such as glass fiber and carbon fiber, has been done widely in commercial PEEK grades to economically enhance the mechanical strengths of PEEK further. Fiber-reinforced PEEK offers a greatly reduced expansion rate and higher bending modulus and has been considered one of the most promising and fastest-growing engineering materials [3].

Like other thermoplastics, PEEK's thermal and mechanical properties are highly dependent on the degree of crystallinity and micro-

morphology [4,5]. The crystallization of PEEK neat resin has been systematically investigated by differential scanning calorimetry [6–10]. Kinetics models have been developed to describe and predict the crystallization of PEEK under isothermal and non-isothermal conditions [7, 8]. Due to limitations of the low cooling rate of conventional differential scanning calorimetry (DSC) and hot stage, those studies were mainly conducted at high crystallization temperatures or with low cooling rates. With the advent of fast scanning calorimetry (FSC), crystallization of thermoplastics [1,11–17], including PEEK, at low crystallization temperature and fast cooling rates can be followed. See et al. have successfully described the isothermal crystallization of three different molecular weight PEEK commercial grades with the Hoffman-Lauritzen crystallization model [1].

For fiber-reinforced PEEK composites, most of the published works focused on crystallization at high crystallization temperatures [18–21]. Fibers may have different roles in affecting the crystallization of PEEK. In most cases, carbon fibers provide a nucleating surface to accelerate the crystallization of PEEK via transcrystallization, where the fiber surface is an effective nucleating site for the resin matrix and

E-mail address: amh234@psu.edu (A.M. Rhoades).

<sup>\*</sup> Corresponding author.

<sup>&</sup>lt;sup>1</sup> Equal contribution.

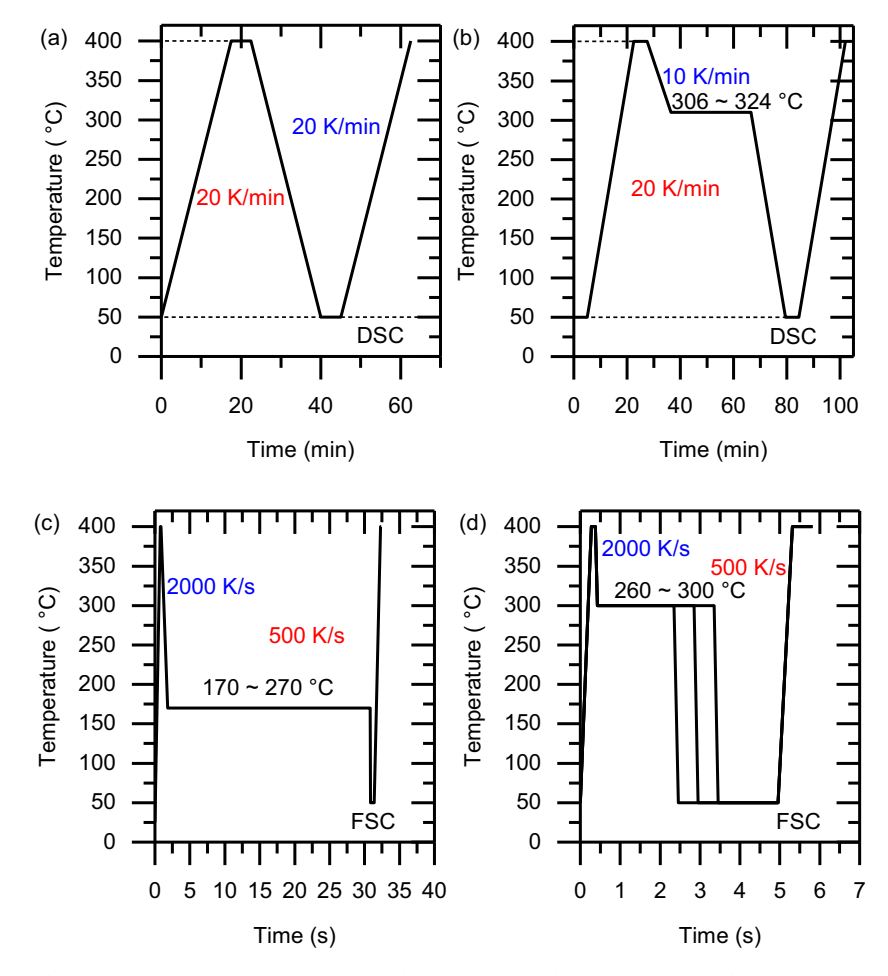


Fig. 1. Temperature-time protocol used for (a) melting-crystallization-remelting in the DSC, (b) isothermal crystallization in the DSC, (c) isothermal crystallization for direct peak time measurement in the FSC and (d) isothermal crystallization with various predefined crystallization times in the FSC, followed by measuring the melting endotherm at 500 K/s (the indirect method).

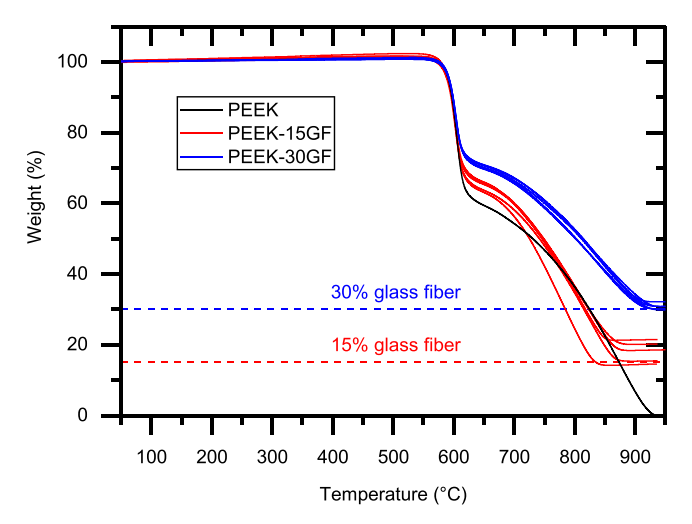


Fig. 2. TGA comparison of PEEK, 15 wt% and 30 wt% glass-fiber-filled PEEK 450 G, each at a heating rate of 20 K/min. In each scan, the gas was switched from  $N_2$  to air at 600 °C.

impingement between neighboring nuclei forces the crystallization to grow normal to the fiber surface [18,22]. Chen and Hsiao attributed the occurrence of transcrystalline interphase in PEEK composites to an epitaxial effect [22]. For glass-fiber reinforced PEEK, observation varies with the surface treatments of glass fiber or commercial PEEK grades.

Poly(p-phenylene terephthalamide) (PPDT)-coated glass fiber reinforced PEEK was found to have transcrystallization [22], while for some commercially available grades, PEEK with glass fiber exhibits slower crystallization kinetics compared to neat resin [19-21]. Regardless, those works suggest that the kinetics model of PEEK neat resin cannot be directly used for predicting the processing and performances of PEEK composites. Although FSC has achieved great success in characterizing neat thermoplastic resins, no work has been done previously on characterizing fiber-filled composites to the best of the authors' knowledge. One possibility is that the reproducibility of this technique in investigating composites is unproven due to the small sample size. The typical sample thickness required for FSC is less than 20 µm for sufficient cooling and heating but is comparable to the fiber diameter, which may lead to filler inhomogeneity in test specimens. Thus, sample preparation needs to be performed with particular attention when using FSC. Furthermore, a systematic investigation of how FSC preparation affects the results is highly desired.

This work studied neat PEEK resin and two commercially available glass fiber-filled PEEK composites, PEEK with 15 wt% and 30 wt% glass fiber. Bulk properties, including glass fiber content, melting, and crystallization properties, were characterized using thermogravimetric analysis (TGA) and DSC. The interior structure of PEEK composites, such as volume fractions of each component, glass fiber parameters, and glass fiber dispersion within PEEK composites, were investigated using X-ray computed tomography (XCT) to follow the inhomogeneity within the composites. XCT is a non-destructive technology that allows accurate interior image reconstruction within solid objects. Given the high spatial

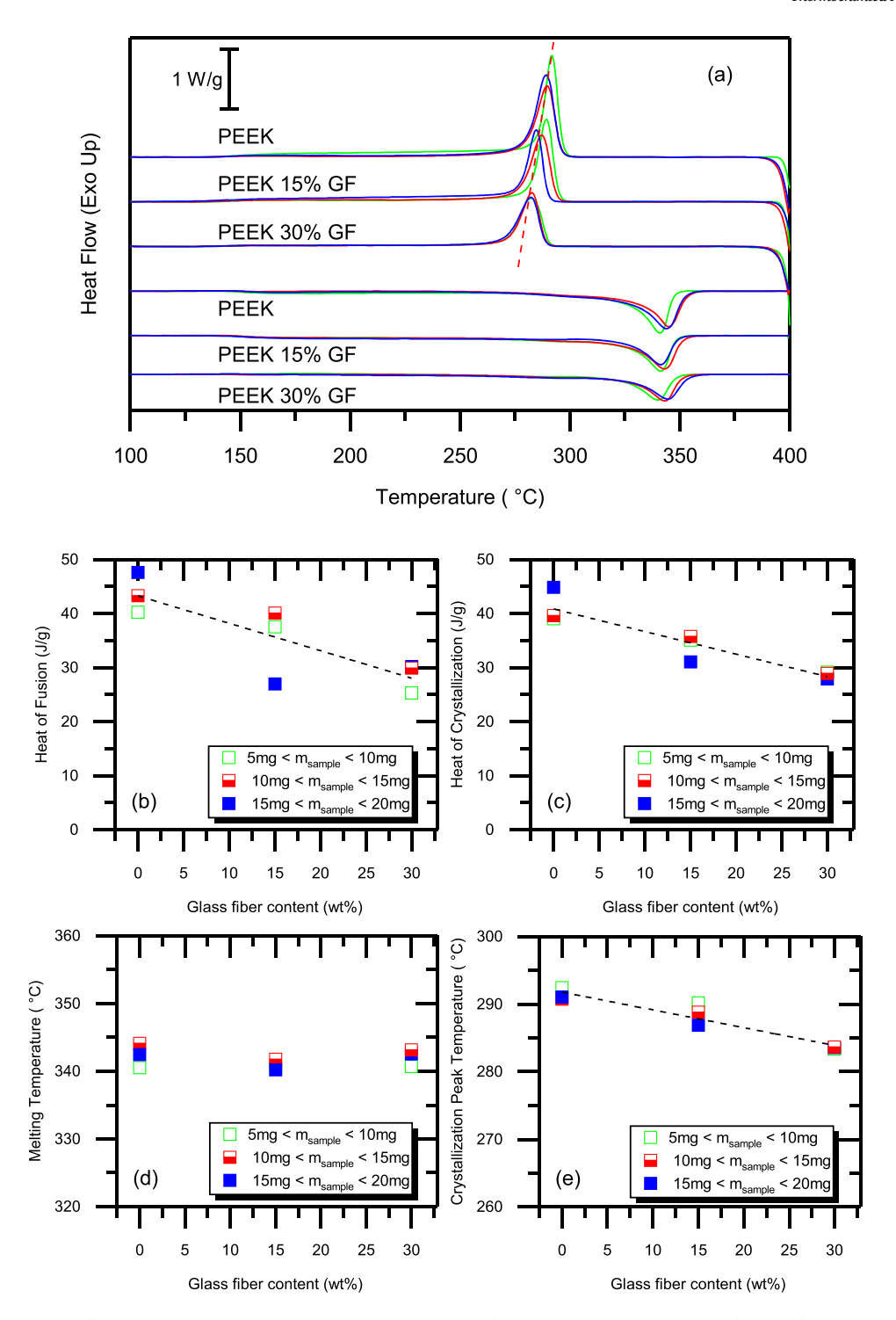


Fig. 3. (a) DSC melting and crystallization curves (exo up) of neat PEEK, PEEK-15GF, and PEEK-30GF using 20 K/min cooling and heating rates. Impact of glass fiber content on (b) specific heat of fusion, (c) specific heat of crystallization, (d) melting temperature, and (e) crystallization peak temperature of PEEK composites with different sample masses. Linear regression lines calculated using data from all mass categories of all grades are added in (b) (c), and (e).

resolution and ability to precisely differentiate multiple phases, XCT has been widely used for fiber-reinforced polymer or other anisotropic materials [23]. Additionally, software such as Avizo and MATLAB enable us to better visualize, manipulate and understand the XCT data. Using reconstructed XCT data, PEEK samples sliced with different directions and frequencies were analyzed to mimic FSC sample preparation. XCT results were validated later by isothermal crystallization of PEEK and its composites using FSC. Lastly, the application of different thermal analyses was confirmed to be feasible in determining the

kinetics of composite materials such as PEEK with glass fiber.

# 2. Experimental section

# 2.1. Materials and preparation

Commercial grade VICTREX PEEK 450G neat resin, VICTREX PEEK 450G with 15 wt% glass fiber (PEEK-15GF), and VICTREX PEEK 450G with 30 wt% glass fiber (PEEK-30GF) were used for the study of PEEK

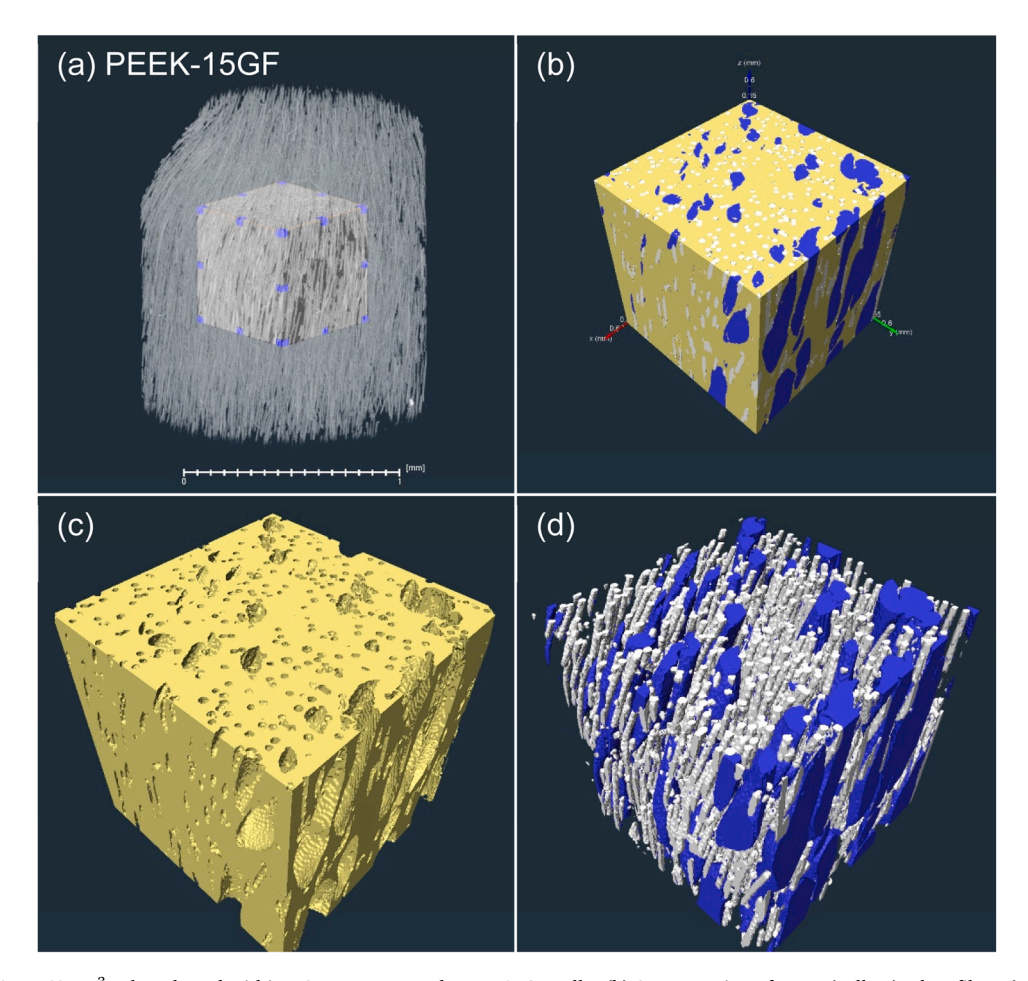


Fig. 4. (a)  $560 \times 560 \times 560 \times 560 \ \mu m^3$  cube selected within XCT reconstructed PEEK-15GF pellet (b) Segmentation of PEEK (yellow), glass fibers (white), voids (blue) (c) matrix of PEEK (d) matrix of glass fibers and voids.

composites crystallization. PEEK 450G neat resin is an injection molding and extrusion grade with a melt flow index of 0.85 g/min at 380  $^{\circ}$ C utilizing a 5 kg gravimetric weight. The number-average molecular weight (Mn = 12,800 g/mol), and polydispersity index (Mw/Mn = 2.9) were measured in a previous publication [1].

#### 2.2. Measurements

Thermogravimetric analysis (TGA) TGA analyses were conducted on a TA SDT Q600 at a heating rate of 20 K/min. A total of five measurements per grade were performed to obtain a mean value and standard deviation. The temperature was scanned from 30  $^{\circ}\text{C}$  to 600  $^{\circ}\text{C}$  under nitrogen gas. Above 600  $^{\circ}\text{C}$  till 950  $^{\circ}\text{C}$ , nitrogen gas was switched to air to completely burn out carbon residue. Measurements were carried out with a 50 mL/min gas flow rate.

Differential Scanning Calorimetry (DSC) DSC analyses were performed with a Mettler-Toledo DSC3 under nitrogen atmosphere. Pellets were cut into three mass categories (5–10 mg, 10–15 mg, and 15–20 mg). For non-isothermal characterization as illustrated in Fig. 1 panel (a), the initial samples were heated at 20 K/min to 400 °C and held for 5 min to erase the previous thermal history; they were further cooled at 20 K/min to 50 °C, held at 50 °C for 5 min, and then heated at the designated rate of 20 K/min. For isothermal crystallization as illustrated in Fig. 1(b), thermal history was erased following the same procedure used in nonisothermal characterization. Then, the temperature was brought down to the designated crystallization temperature at a rate of 20 K/min and then held for a time long enough to observe the crystallization. The sample was then cooled to 50 °C at a rate of 20 K/min and held there for 5 min before being heated back to 400 °C and annealed. This procedure

was repeated over the crystallization temperature range from 306  $^{\circ}\text{C}$  to 324  $^{\circ}\text{C}.$ 

Fast Scanning Calorimetry (FSC) Calorimetric analyses on a FSC chip were carried out using a Mettler Toledo Flash DSC 1 connected to a Huber TC100 two-step cooling intracooler. FSC sensors were conditioned and corrected before loading the specimen. Dry nitrogen gas was used to purge the calorimeter. The pellets were microtomed to obtain sections with a thickness of 12  $\mu m$  perpendicular to the extrusion direction of the pellets. These thin sections were cut to obtain a lateral dimension of around 50 - 100  $\mu m$ , using a scalpel under a Leica stereomicroscope. Thin specimens were directly loaded on the chip.

For determination of FSC sample mass, the same thermal history was introduced to samples in DSC and FSC by cooling at 20 K/min (0.33 K/s) from 400 °C to 50 °C following a similar method introduced by Poel et al. [24]. Regardless of the heating rates used in DSC and FSC, the melting enthalpy is proportional to the sample mass. FSC sample mass,  $m_{FSC}$ , is then calculated by  $m_{FSC} = \frac{\Delta H_{m,FSC}}{\Delta H_{m,DSC}} m_{DSC}$ .  $\Delta H_{m,FSC}$  and  $\Delta H_{m,DSC}$  are the melting enthalpies in units of J, measured by the FSC and DSC, respectively, and  $m_{DSC}$  is the DSC sample mass.

For obtaining kinetics information, PEEK neat resin and its composites were initially heated to 400 °C (higher than the reported  $T_m^0$  of PEEK, 380.5 °C [1]) to erase thermal history. Then, the melt was cooled to the crystallization temperature at a rate of 2000 K/s. The sample was kept at the selected isothermal crystallization temperature for 30 s to follow crystallization. Crystallization peak time was directly measured from the exothermic peak time. The experimental protocol is summarized in Fig. 1 panel (c).

An indirect method by measuring the heat of fusion after a

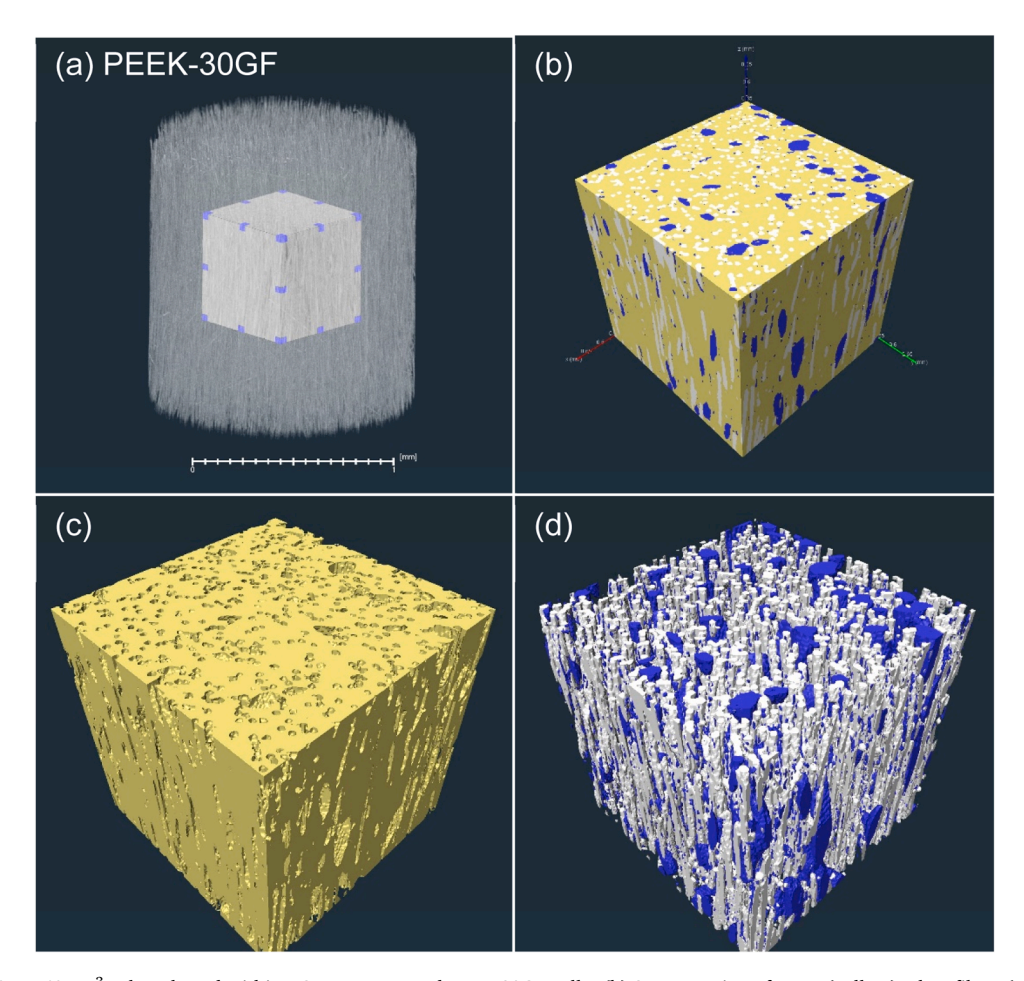


Fig. 5. (a)  $560 \times 560 \times 560 \times 560 \ \mu m^3$  cube selected within XCT reconstructed PEEK-30GF pellet (b) Segmentation of PEEK (yellow), glass fibers (white), voids (blue) (c) matrix of PEEK (d) matrix of glass fibers and voids.

predefined crystallization time was used to estimate crystallization peak time in the temperature region between 260 - 300 °C as displayed in Fig. 1 panel (d) [11]. The quenching rates used in this research were proven to be fast enough to bypass the melt-crystallization of PEEK [1].

X-ray computed tomography (XCT) A Zeiss Xradia Versa 620 was used for the XCT scan of the pellets. A voxel size of 700 nm and 16 bits per pixel was selected. For each pellet, approximately,  $2000 \times 2000 \times 2000$ slices were taken with an exposure time of 0.7 s. For data size reduction, a MATLAB code (SI Appendix 1) is used to consolidate every  $4 \times 4 \times 4$ voxel into 1 coarser voxel. The coarser voxel is still small compared with the fiber diameter (shown below to be of order 10 µm). As displayed in Fig. SI 1, the data size reduction has a negligible effect on the identification of glass fiber and voids. 3D models were reconstructed using Avizo by Thermo Fisher Scientific. Prior to any detailed analyses, Avizo median filter and non-local means filter were applied to enhance the contrast between different components and mitigate the potential effects from artifacts. A segmentation module from Avizo was then employed to distinguish the polymer matrix, voids, and glass fibers. The fibers within the specimen were identified, isolated, and reconstructed using the Avizo fiber tracing module. The fiber and void contents were measured in three directions using Avizo Global analysis module.

#### 3. Results and discussion

# 3.1. Characterization of PEEK and its composites using TGA and DSC

The content of glass fiber in PEEK composites was first characterized using TGA, as displayed in Fig. 2. The sample was run under nitrogen flow to follow the first step of thermal degradation near  $560\,^{\circ}$ C, due to

random chain scission of the ether and ketone bonds followed by volatilization [25]. At a temperature of 600 °C, gas was switched from  $N_2$  to air to completely burn out the polymer residual. A glass fiber content of  $18\pm3\%$  and  $31\pm1\%$ , for PEEK-15GF and PEEK-30GF, respectively, was determined from the residue weight percentage. Both samples have their average glass fiber contents slightly higher than the expected values. Apart from the average fiber content, PEEK-15GF has a larger variation in the glass content than its 30GF counterpart, presumably due to less uniform dispersion of the glass fiber.

The effect of glass fiber on the crystallization and melting behaviors of neat PEEK and PEEK composites was then evaluated by DSC using constant rate scanning. Three mass categories were studied as described in the experimental section. Measured thermal properties are summarized in Table SI 1. As displayed in Fig. 3 panel (a), no major difference was obtained in crystallization and melting curves, suggesting the sample mass used for DSC barely has any impact in the sample mass range studied. The effect of glass fiber content on the heat of fusion, the heat of crystallization, crystallization temperature, and melting temperature values are summarized in Fig. 3 panels (b) – (e). The specific heat of fusion and specific heat of crystallization decrease with higher glass fiber content, since PEEK resin is the only crystallizable component in composites. Assuming glass fiber content in PEEK-15GF and PEEK-30GF is 15% and 30%, PEEK, PEEK-15GF, PEEK-30GF have a degree of crystallinity of 33.6%, 31.5%, 31.3%, respectively, using 130 J/g for PEEK's crystalline heat of fusion [10]. The melting temperature of all samples show negligible difference, while the crystallization temperature decreases with higher glass fiber content. This work suggests, in the used commercial grades, the glass fibers act like obstacles rather than nucleants, as suggested by a lower crystallization temperature at higher

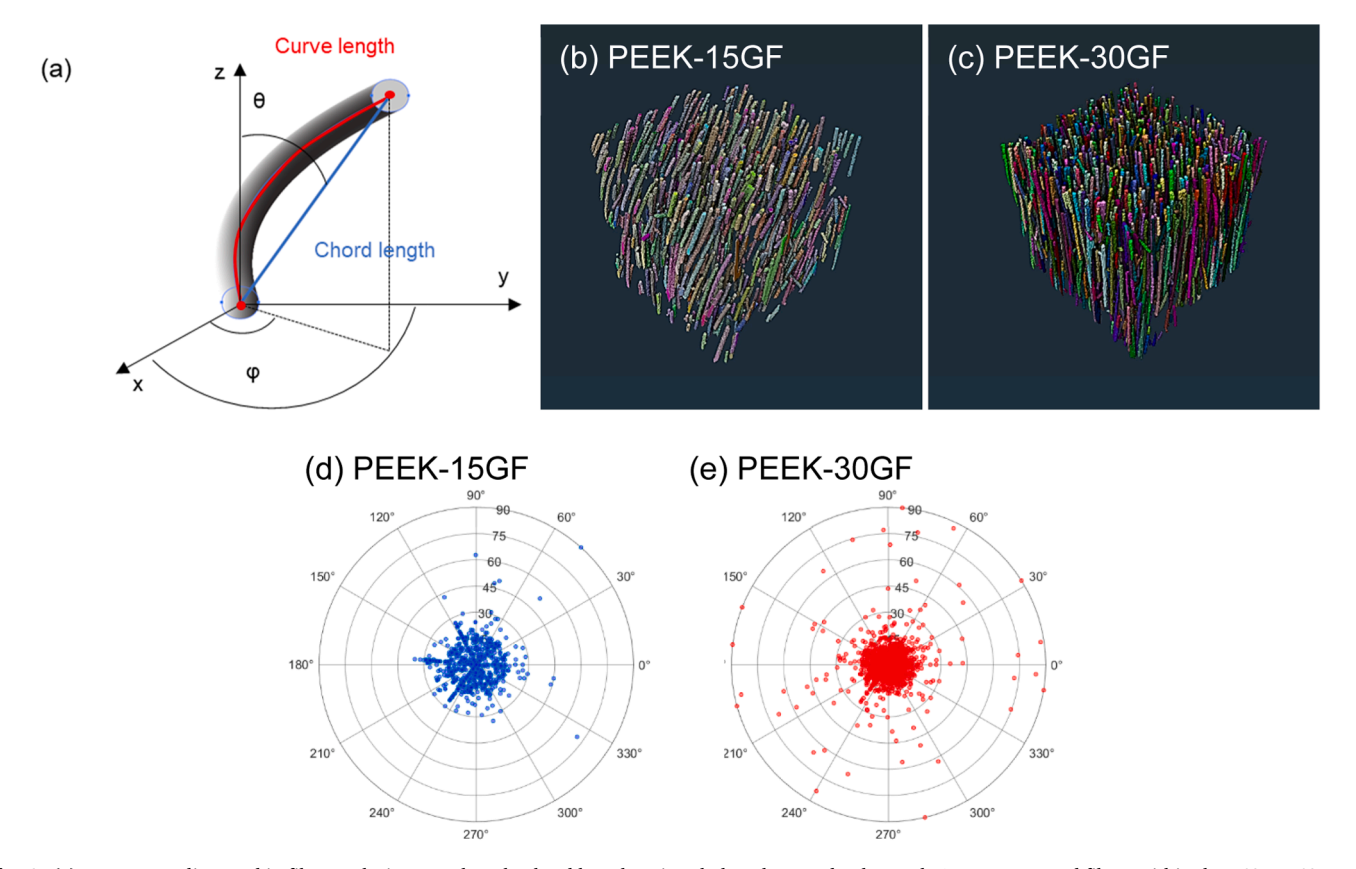


Fig. 6. (a) Parameters discussed in fiber analysis: curve length, chord length, azimuthal angle  $\varphi$ , and polar angle  $\theta$ . Reconstructed fibers within the 560  $\times$  560  $\times$  560  $\times$  560  $\times$  mm<sup>3</sup> cube for (b) PEEK-15GF and (c) PEEK-30GF. Scatter polar plot of fiber orientation distribution with azimuthal angle  $\theta$  and polar angle  $\varphi$  for (d) PEEK-15GF and (e) PEEK-30GF.

glass fiber content. These conclusions agree with previous studies in other glass-fiber-filled PEEK grades [19–21].

# 3.2. X-ray computed tomography analysis

Fast scanning calorimetry is the technique that enables the crystal-lization kinetics studied under processing-relevant conditions. However, the FSC characterization on composites meets some challenges because of the requirement of using a small sample size: component inhomogeneity is more significant when the sample size is comparable to the filler size. To understand how different ways of FSC sample preparation can potentially affect the results, volume and distribution information of each component, such as resin, filler, and impurities, was investigated by XCT.

A  $560 \times 560 \times 560 \, \mu m^3$  cube in the center of the XCT scanned pellet was extracted for the subsequent analysis to avoid surface defects of the pellets on data analyses, as illustrated in panel (a) of Figs. 4 and 5. As displayed in panels (b)(c)(d) of Figs. 4 and 5, the three components of the composites, resin, glass fibers, and voids, were marked with different colors. Fibers, as well as the voids, have mostly aligned or stretched along the z-direction, suggesting the glass fibers help to induce the flow of micro-voids. Surprisingly, the void content and size of embedded voids between fibers in PEEK-15GF appear to be *larger* than its 30GF counterpart. This observation is supported by the measured volume fraction, where the void volume percentage is 30.8% in PEEK-15GF and 10.4% in PEEK-30GF. On the contrary, resin volume percentage 63.7% in PEEK-15GF is lower than 72.2% in PEEK-30GF.

According to the literature, PEEK resin and glass fiber have a density of 1.3 g/cm<sup>3</sup> and 2.5 g/cm<sup>3</sup> [26,27]. Assuming the void has a density of 0 g/cm<sup>3</sup>, the sample mass W of the cube can then be estimated using the formula  $W = \sum_i \rho i V_i$ , where  $\rho$ i and  $V_i$  are the density and volume fraction

of each component *i* within the cube. The cube for PEEK-15GF and PEEK-30GF has a weight of 0.17 mg and 0.24 mg, respectively. Although both numbers are much lower than the amount of sample used for TGA and DSC characterization in the previous section, the calculated weight percentage values of glass fiber in each cube, 14.32% for PEEK-15GF and 31.73% for PEEK-30GF, are close to their expected glass fiber contents. Thus, XCT volume analysis of the cube suggests relatively good component homogeneity in typical TGA and DSC samples.

Information associated with the fibers within the composites was further extracted in regard to fiber diameter, length, and orientation, as displayed in Fig. 6 and summarized in Table SI 3. As displayed in Fig. 6 panels (b) and (c), 780 and 1632 fibers were identified and analyzed in PEEK-15GF and PEEK-30GF, respectively. Diameter values of glass fibers in both composites were found to be close to 10  $\mu m$ . Similar glass fiber diameter confirms that the method used in XCT can effectively avoid possible dilation, which can mistakenly count two or more fibers as one fiber. In addition, two types of fiber length values, fiber chord length and curve length, were measured as illustrated in Fig. 6 panel (a). Due to the rigid structure of glass fiber, the ratio of chord length and curve length is nearly 1, which again confirms good isolation of glass fibers. The measured number-average fiber chord length in PEEK-30GF is 165  $\mu m$ , which is 43% longer than the number-average fiber chord length of 115  $\mu m$  in PEEK-15GF.

Fiber orientation within the pellets was characterized by azimuthal angle  $\phi$  in the x-y plane with a value between 0 and 360° and polar angle  $\theta$  from the z-axis with a value between 0 and 90° in the spherical coordinate system, as illustrated in Fig. 6 panel (a). Polar plots, as shown in Fig. 6 panels (d) and (e), summarize the azimuthal angle  $\phi$  and polar angle  $\theta$  of glass fibers in PEEK-15GF and PEEK-30GF. For azimuthal angle  $\phi$ , both samples do not show any preferred angle from the polar plot. For the polar angle  $\theta$ , most fibers flow aligned within 15° from the

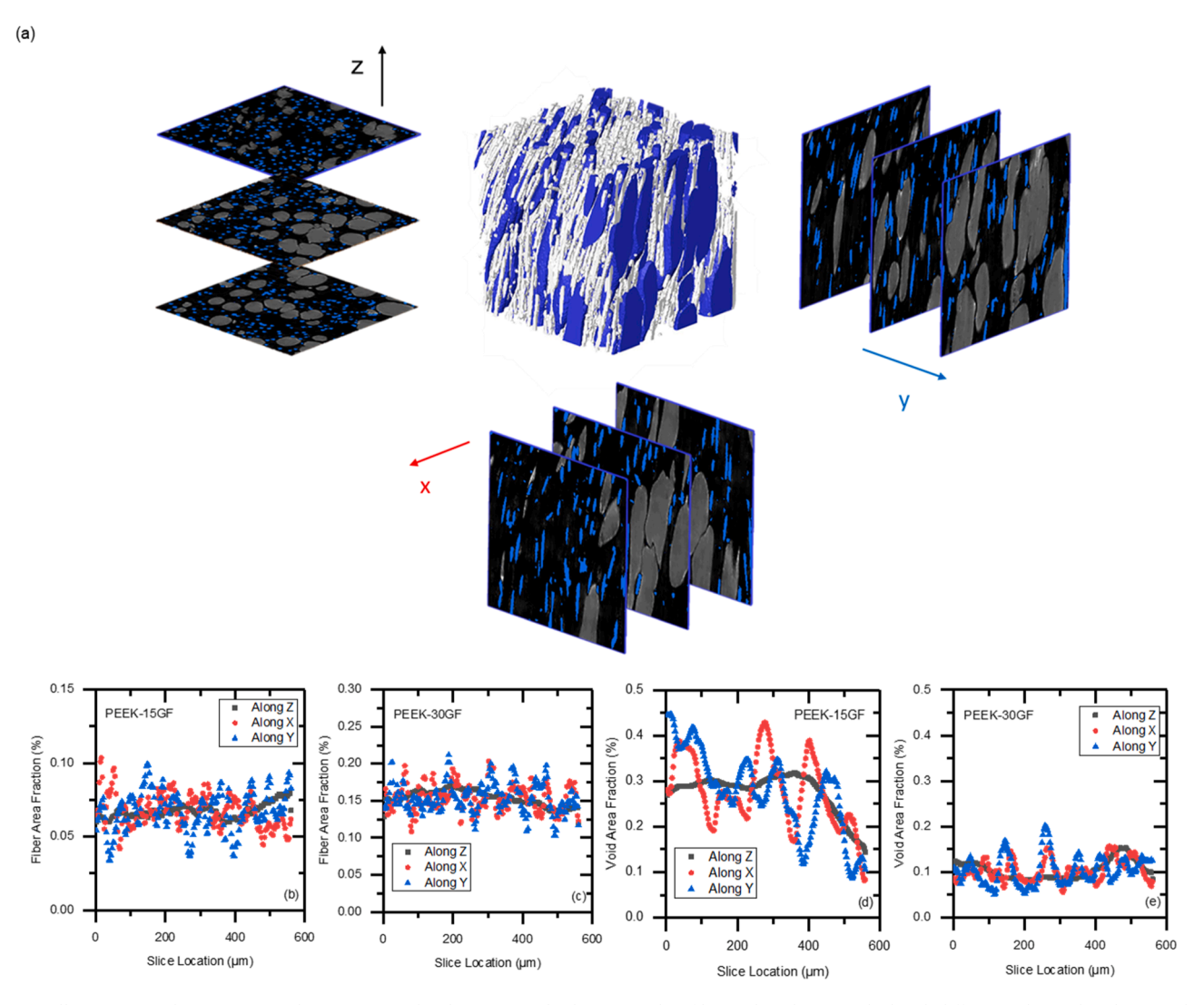


Fig. 7. (a) Illustration on slicing segregated PEEK-15GF cube along x, y, and z direction. Glass fiber and voids are marked with different colors. Fiber (b) (c) and void (d) (e) area fraction along the slice location in PEEK-15GF and PEEK-30GF with a sampling frequency of every 2.8 μm.

z-axis for both composites studied. Hermans orientation factor f, according to the formula  $f=\frac{3\cos^2\theta-1}{2}$ , is 0.89 and 0.92 for PEEK-15GF and PEEK-30GF, respectively. A slightly higher Hermans orientation factor in PEEK-30GF than in PEEK-15GF agrees with the observation in Fig. 6 (b) and (c), that glass fibers in PEEK-30GF are better aligned.

The volume segmentation and fiber analyses show that PEEK-15GF has more voids, shorter fiber length, and less aligned fibers along the z direction compared to PEEK-30GF. This observation is consistent with the previous observation in TGA that PEEK-15GF sample has more data variation than PEEK-30GF.

XCT reconstructed cube with segregated compounds gives an excellent opportunity to simulate how sample preparation in FSC affects the homogeneity of glass fiber. Area fractions of each component along three slice directions were evaluated, as illustrated in Fig. 7 panel (a). The cube was sliced at a sampling frequency of 2.8 µm for measuring area fractions of PEEK, glass fiber, and voids. When slicing parallel to the x-y plane, i.e., the microtome advancing in the z-direction, each slice is perpendicular to the glass fiber flow direction, which mainly shows the round cross-section of glass fibers as shown in Fig. 7 panel (a). When slicing parallel to the x-z or y-z planes, i.e., the microtome advancing in the y-direction or x-direction, respectively, each slice is parallel to the glass fiber flow direction.

Fiber and void area fractions along three slice directions with a sampling frequency of 2.8  $\mu m$  in PEEK-15GF and PEEK-30GF are

compared in Fig. 7 panels (b) - (e). Fiber area fraction along the z-slice direction always showed much less variation than in the x- and y-slice directions. For void area fraction, data variation appears to be more significant.

The fiber weight fraction was calculated along three directions, as shown in Fig. 8 panels (a) and (b). At a sampling frequency of 2.8  $\mu m$ , both samples had their glass fiber weight fraction near 15% and 30% only along the z direction. Fiber weight fraction W% using a larger sampling size was calculated by averaging all the data within the sampling range collected initially using 2.8  $\mu m$  sampling frequency. When the sampling frequency changes to a higher value, no significant change of data variation is found along the z direction, while glass fiber weight content consistency along the x and y direction is greatly improved. When the sampling frequency reaches 22.4  $\mu m$ , glass fiber weight content along all directions is near the expected value in bulk.

A detailed evaluation of how sampling size in a range from 2.8 to 47.6  $\mu m$  affects the coefficient of variation (CV) is performed in three directions for both samples, as displayed in Fig. 8(c) and (d). The CV is defined as the ratio of standard deviation  $\sigma$  to the mean  $\mu$  of glass fiber weight fraction. In both samples, the CV value suggests glass fiber weight consistency is always better by slicing perpendicular to the fiber flow direction. The CV value for z direction cannot be significantly improved when the sampling size is 5.6  $\mu m$ , slightly smaller than the measured fiber diameter of 10  $\mu m$ . The CV value along the x and y direction

X. Zhang et al.

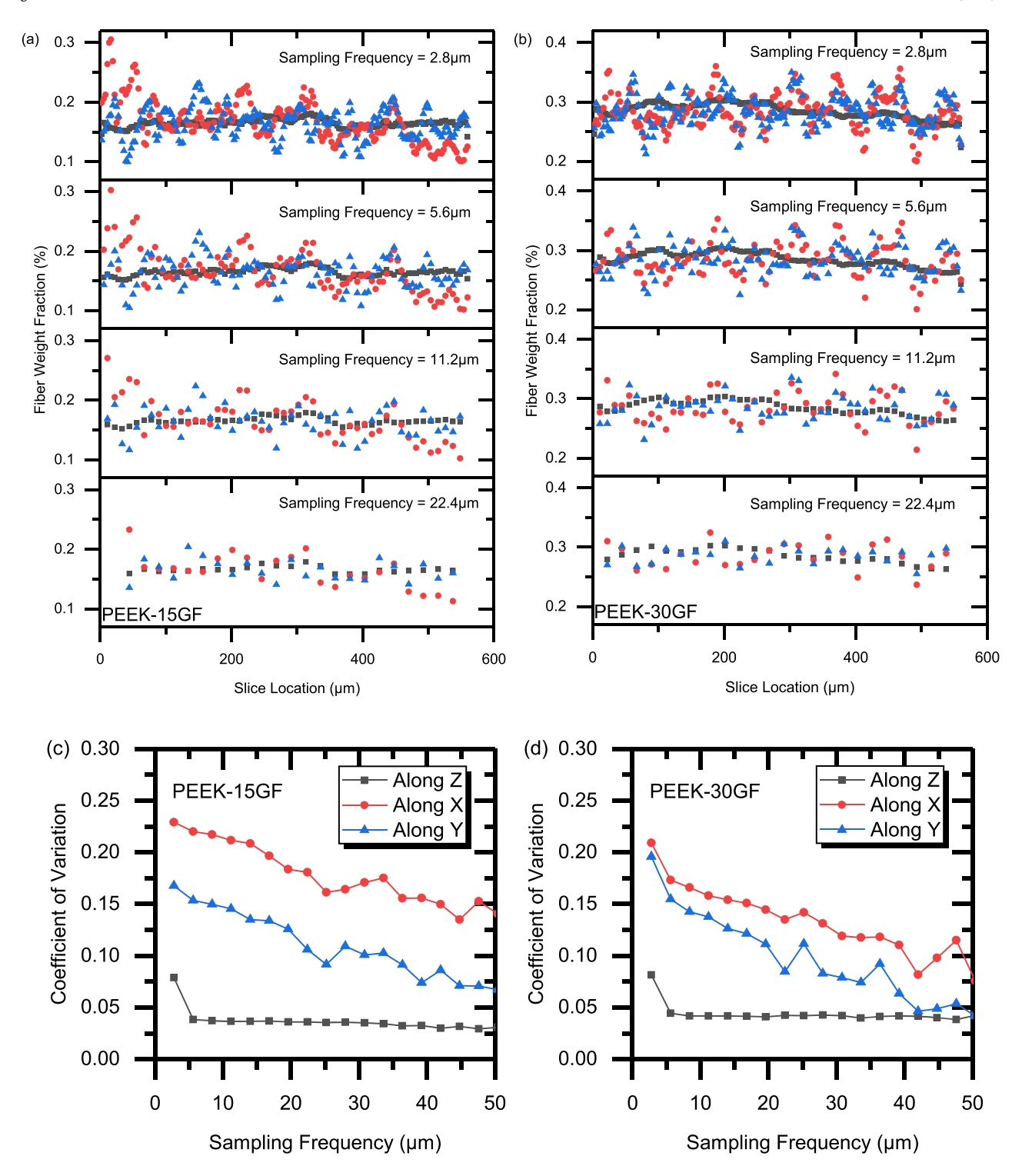


Fig. 8. The fiber weight fraction of (a) PEEK-15GF and (b) PEEK-30GF with various sampling frequencies. Data measured along z (perpendicular to fiber flow direction), x and y slice directions (along fiber flow directions) are marked with  $\blacksquare$ ,  $\bullet$ , and  $\blacktriangle$  symbols, respectively. Coefficients of variation along z, x, and y directions with sampling frequency from 2.8  $\mu$ m to 47.6  $\mu$ m in (c) PEEK-15GF and (d) PEEK-30GF. The coefficient of variation is defined as the ratio of standard deviation  $\sigma$  to the mean  $\mu$  of glass fiber weight fraction.

gradually decreases with a larger sampling size. At the sampling frequency of 47.6  $\mu m$ , slicing along the z direction is still better than along the x and y directions. Comparing PEEK-15GF and PEEK-30GF, both samples have similar CV values along the z direction, and PEEK-30GF generally has lower CV values in the x and y direction. This observation can be interpreted by the lower dispersion of glass fiber and lower void volume variation in PEEK-30GF than in PEEK-15GF.

The XCT slicing analysis suggests that in FSC sample preparation, the sample should be microtomed perpendicular to the fiber flow/extrusion direction. A sample thickness comparable to the glass fiber diameter or higher should provide a reasonably good consistency in glass fiber content for the FSC sample. On the other hand, for a typical FSC sample size ( $<50~\mu m$ ), the sample being microtomed along the extrusion direction likely will have a larger data variation.

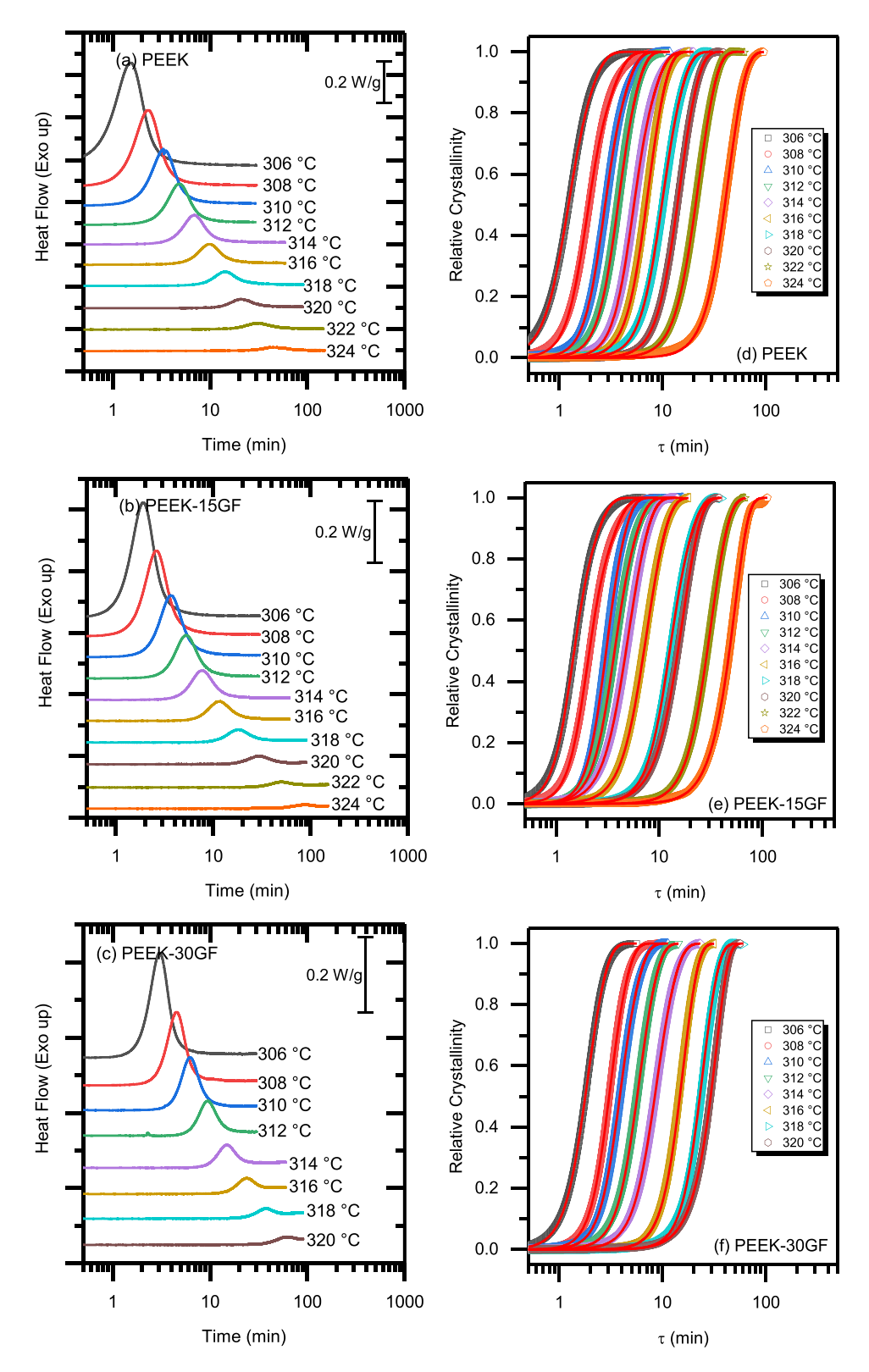


Fig. 9. DSC isothermal crystallization exotherms of (a) PEEK, (b) PEEK-15GF, and (c) PEEK-30GF at indicated temperatures after cooling at 20 K/min from 400 °C. The modified Avrami model (Eq. (1)) fitted to isothermal crystallization kinetics of (d) PEEK, (e) PEEK-15GF, (f) PEEK-30GF at indicated temperatures.

# 3.3. Crystallization kinetics

The crystallization kinetics of PEEK and its composites was first investigated by isothermal crystallization in the low undercooling region between 306 - 324  $^{\circ}$ C using DSC. Representative isothermal crystallization curves are displayed in Fig. 9(a) (b) (c) with their

corresponding relative crystallinity evolutions plotted against crystallization time,  $\tau$ , which is defined as the time after induction time  $t_0$ . All curves were then fitted with the modified dual Avrami equation by Seo et al. [1],

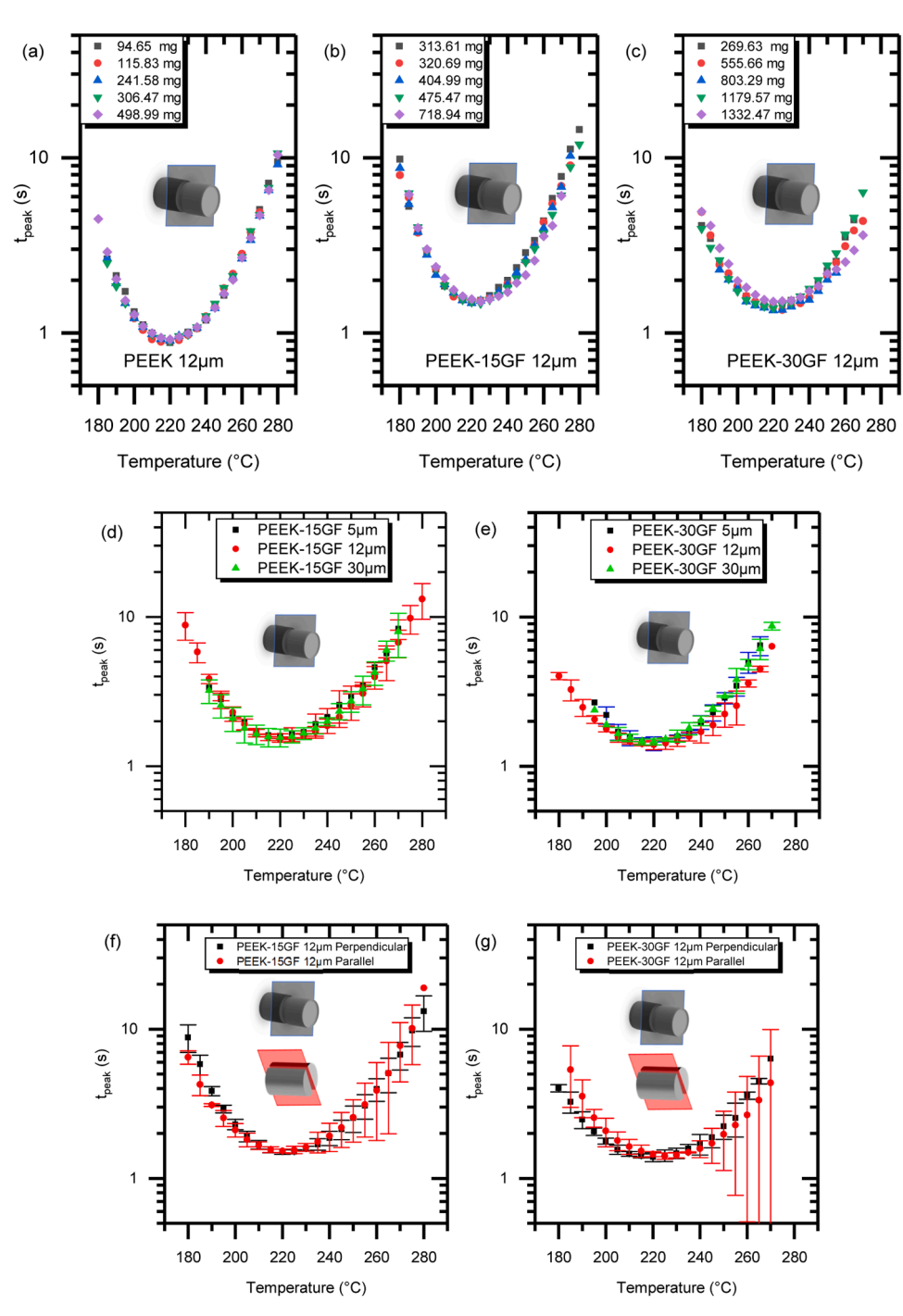


Fig. 10. Crystallization peak time  $t_{peak}$  of (a) PEEK, (b) PEEK-15GF, and (c) PEEK-30GF with 12  $\mu$ m thickness but various lateral sizes cut perpendicular to the fiber direction.  $t_{peak}$  of (d) PEEK-15GF and (e) PEEK-30GF with various thicknesses cut perpendicular to the fiber direction.  $t_{peak}$  of (f) PEEK-15GF and (g) PEEK-30GF with different microtomed directions. Illustrations of microtome direction are added as inset.

$$\emptyset(\tau) = \frac{1 - \exp(-k_p \tau^{n_p})}{1 - \exp(-k_p \tau^{n_p}) + \exp\left(-k_p \tau^{n_s} \left(\frac{-\ln(0.5)}{k_p}\right)^{1 - \left(\frac{n_s}{n_p}\right)}\right)}$$
(1)

where  $\varnothing(\tau)$  is the relative crystallinity at the crystallization time  $\tau$  ( $\varnothing$ —1 as  $\tau$ — $\infty$ );  $k_p$  is the primary crystallization rate constant;  $n_p$  is the primary crystallization Avrami exponent; and  $n_s$  is the secondary crystallization Avrami exponent. The overall heat of fusion of crystallization for a given temperature was measured to normalize the crystallization exotherm. Crystallization peak time,  $t_{peak}$ , and half transformation time,  $t_{0.5}$ , were determined using this model.

The same set of data was also fitted using the classic Avrami (KJMA) model [28,29] as displayed in Fig. SI 2. It is noted that the modified Avrami equation offers a better fitting quality compared to the original Avrami equation because the modified Avrami equation takes secondary crystallization into account. As summarized in Fig. SI 3, all three grades have their Avrami index n near 3, similar to the previous study by Cebe and Hong [6], suggesting they all follow the heterogenous nucleation mode.

FSC experiments were carried out to extract crystallization kinetics at higher undercooling conditions. For exothermic curves that show high signal-to-noise ratio, crystallization peak times were directly measured from exothermic peaks during isothermal crystallization in

the temperature region between 180 and 280 °C. Samples microtomed perpendicular to the fiber direction were first examined, and the standard microtome thickness was controlled to be 12  $\mu$ m. Five samples covering a large sample range were collected per grade to evaluate the data variation. No major lateral size effect was found between those samples, as seen in Fig. 10(a) (b) (c).

To evaluate the thickness effect, FSC data of PEEK-15GF and PEEK-30GF with 5  $\mu m,~12~\mu m,$  and 30  $\mu m$  thickness were compared, as displayed in Fig. 10(d) (e). No clear impact from the thickness was found in those data. This conclusion agrees with the discussion from XCT that the consistency of glass fiber content for slicing perpendicular to the fiber direction remains basically unchanged when the sampling thickness is 5.6  $\mu m$  or higher.

As shown in Fig. 10(f) (g), although a similar peak time was observed for the same grade with different microtome directions, a larger error bar was found in samples microtomed along the fiber flow direction. This observation agrees with the XCT conclusion that at a thickness of 12  $\mu m$ , significant fiber inhomogeneity still exists if the microtome direction is not perpendicular to the flow direction.

Isothermal crystallization kinetics of PEEK and its composites in the temperature region above  $270~^{\circ}\text{C}$  or higher temperatures are not measurable from the FSC exotherm peak due to a weak signal-to-noise ratio. Instead, crystallization peak time was measured by an indirect method, as shown in Fig. 11.

Due to the prolonged crystallization time, secondary crystallization greatly contributes to the measured heat of fusion  $\Delta H_m$  values. Normalization by the final measured heat of fusion value, as previously done in Avrami and modified Avrami methods, will inevitably overestimate the half-transformation time. Zhuravlev et al. [30–32] proposed a new model that considers both primary crystallization and secondary crystallization to describe the heat of fusion change during annealing, as follows,

$$\Delta H_{\rm m} = \Delta H_{\rm m,max} \left\{ 1 - \exp\left[ -\left(\frac{\tau}{\tau_{0.5}} \ln 2\right)^n \right] \right\} + A_2 [\ln(\tau) - \ln(\tau_{0.5})] \left[ 0.5 \left(\frac{|\tau - \tau_{0.5}|}{\tau - \tau_{0.5} + 1}\right) \right]$$
 (2)

where  $\Delta H_{\mathrm{m,max}}$  is the heat of fusion at the end of primary crystallization,  $\tau_{0.5}$  is the half crystallization time after removing the induction time, n is the Avrami index, and  $A_2$  is a secondary crystallization parameter. It should be noted that half crystallization time equals  $\tau_{0.5}$  only when n is 1. For higher n, the fitted  $\tau_{0.5}$  underestimates the half crystallization time. A modified equation is proposed here to fit the measured heat of fusion of PEEK and composites after different crystallization times. This equation also works for other n values.

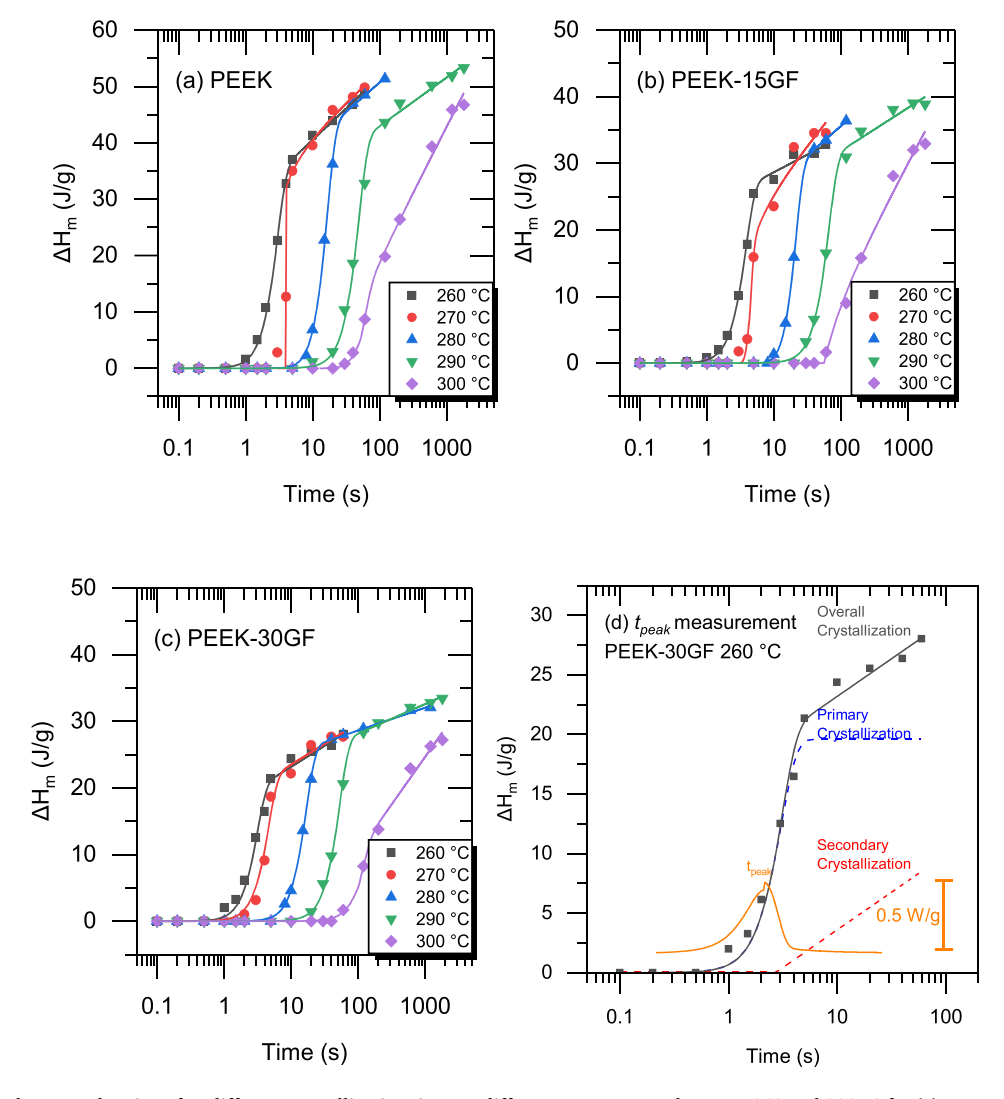


Fig. 11. Heat of fusion change on heating after different crystallization times at different temperatures between 260 and 300 °C for (a) PEEK, (b) PEEK-15GF, and (c) PEEK-30GF. The fitted line from Eq. (2) to isothermal crystallization kinetics are added. (d) Example of  $t_{peak}$  measurement using PEEK-30GF 260 °C.

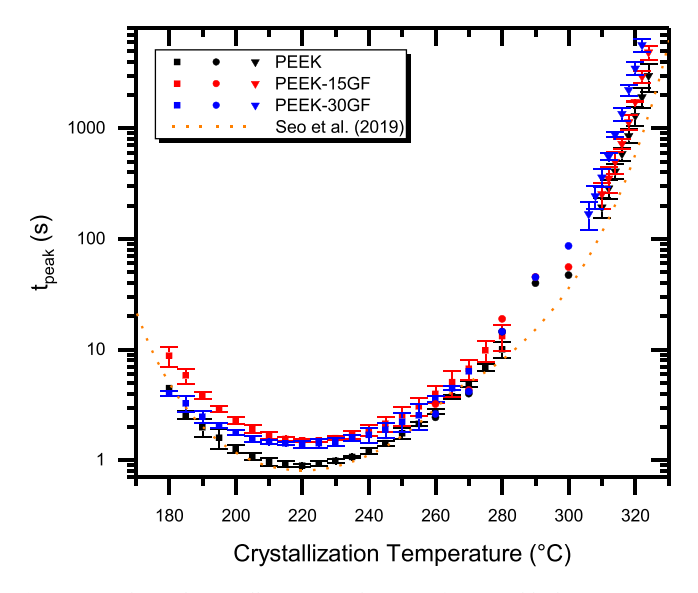


Fig. 12. Isothermal crystallization peak time of PEEK (black), PEEK-15GF (red), and PEEK-30GF (blue). Crystallization peak times collected from FSC exothermic peaks, FSC indirect method, and DSC exothermic peaks are represented by ■, ◆, ▼symbols, respectively. Data for the dashed line is from previous work for unfilled PEEK by Seo et al. [1].

$$\Delta H_{\rm m} = \Delta H_{\rm m,max} \left\{ 1 - \exp \left[ - \left[ \frac{\tau}{\tau_{0.5}} (\ln 2)^{\frac{1}{n}} \right]^n \right] \right\} + A_2 [\ln(\tau) - \ln(\tau_{0.5})] \left[ 0.5 \left( \frac{|\tau - \tau_{0.5}|}{\tau - \tau_{0.5}} + 1 \right) \right]$$
(3)

Since PEEK is known to exhibit unimodal temperature-dependence kinetics across the entire temperature range, as previously reported by Seo et al. [1] and Tardif et al. [33], Avrami index of 3 determined from the DSC region will be used in the equation above as a constant. *t*peak determined from the first derivative of the fitted curve is extracted as illustrated in Fig. 11(d).

The overall isothermal crystallization kinetics associated with crystallization peak time, tpeak, are summarized in Fig. 12. Data collected from three methods show good consistency across the wide temperature range. The PEEK data collected in this study shows good agreement with the previous work by Seo et al. [1]. In both FSC and conventional DSC regimes, there is a noticeable separation in the crystallization time between the neat resin and its composite counterparts, suggesting that glass fibers slow down the overall quiescent crystallization kinetics of PEEK resin. Additionally, an SEM image of PEEK-15GF fracture surface, as displayed in Fig. SI 4, found that fractured glass fiber is free of PEEK resin, suggesting weak adhesion between two components in the composites. This is different from SEM observation in carbon-fiber-filled PEEK, where transcrystallization nucleated by carbon fiber leads to better adhesion between carbon fibers and PEEK resin [34]. The SEM image suggests that the glass fiber used in the studied composites has no nucleation effect. It is known that non-nucleating or weakly nucleating fibers act as obstacles for spherulitic growth and may slow down or completely stop the growth front [35]. Our observation agrees with the previous glass-fiber-filled PEEK composite kinetics studies [19–21]. Even more interesting is the observation that the 30 wt% glass-filled resin at high-to-mid undercooling seems to show faster crystallization compared to PEEK-15GF. As concluded earlier from XCT analysis, PEEK-15GF is suspected of having more processing history than its 30 wt % GF counterpart, as suggested by its significantly larger void volume and lower resin volume fraction. It is believed that crystallization stops when the growth front impinges not only on the glass fiber but also on the void surface. Overall lower resin fraction in PEEK-15GF causes slower crystallization kinetics than in PEEK-30GF. In the conventional DSC region, the data suggests that the crystallization of the 30 wt%

glass-filled resin is slower than the 15 wt% glass-filled resin. One possibility is that voids have a much longer time to coalesce during DSC experiments, so the void slow-down effect on PEEK crystallization becomes less significant. Therefore, their more significant presence would inevitably have a more substantial effect on the crystallization kinetics compared to neat PEEK [35]. Overall, both visible regions distinguish the crystallization kinetics between the neat PEEK resin and its 15 wt% and 30 wt% glass-filled counterparts.

# 4. Conclusions

This work systematically investigates the crystallization kinetics of PEEK and its composites in a wide temperature range. A feasibility study using ultra-small samples for the FSC was carried out.

TGA and DSC were used first to characterize thermal properties in bulk. The interior structure of PEEK composites within a  $560 \times 560 \times 560 \, \mu m^3$  cube was then investigated using XCT. The weight fraction of glass fiber was found to be close to the expected value in both composites. The detailed fiber analysis extracted the fiber information of number, diameter, length, and orientation. Higher void content, shorter fiber length, and lower orientation factor observed in PEEK-15GF suggest additional processing history compared to PEEK-30GF. To mimic FSC sample preparation, the effect of slicing direction and sample thickness on glass fiber inhomogeneity was performed using XCT reconstructed 3D structures of composites. A lower coefficient of variation is observed when the slicing direction is perpendicular to the fiber direction rather than along the fiber direction. The coefficient of variation cannot be further improved if the slicing thickness is comparable to the fiber diameter.

The effects of lateral size, thickness, and microtome direction on crystallization kinetics were studied by FSC. This work confirms that FSC could be a valuable tool for studying the crystallization of fiber-filled composites after carefully controlling the directionality of the fiber within the specimen and sample thickness.

Isothermal crystallization kinetics in a wide temperature range (170 - 324  $^{\circ}\text{C})$  of PEEK and its composites confirms that the non-nucleating glass fibers used in PEEK composites slow down the PEEK crystallization by acting as obstacles to slow down or stop the crystal growth. The slowest crystallization kinetics of PEEK-15GF is believed to be caused by a combined obstacle effect from glass fiber and voids.

#### CRediT authorship contribution statement

Xiaoshi Zhang: Methodology, Formal analysis, Investigation, Writing – original draft, Writing – review & editing. Jason D. Alexander: Methodology, Formal analysis, Investigation, Writing – original draft, Writing – review & editing. Jiho Seo: Investigation, Writing – review & editing. Anne M. Gohn: Investigation, Writing – review & editing. Matthew J. Behary: Investigation. Richard P. Schaake: Resources. Ralph H. Colby: Writing – review & editing, Supervision, Project administration, Resources. Alicyn M. Rhoades: Writing – review & editing, Supervision, Project administration, Resources.

# **Declaration of Competing Interest**

The authors declare no competing financial interest.

#### Data availability

Data will be made available upon reasonable request.

## Acknowledgments

This research was funded by AB SKF and the National Science Foundation Grant 1653629. Our discussions with Gijs de Kort are gratefully acknowledged.

The paper is intended for publication in a special issue of Thermochimica Acta in honor of the scientific work of Professor Bernhard Wunderlich.

## Supplementary materials

Supplementary material associated with this article can be found, in the online version, at doi:10.1016/j.tca.2023.179442.

#### References

- [1] J. Seo, A.M. Gohn, O. Dubin, H. Takahashi, H. Hasegawa, R. Sato, A.M. Rhoades, R. P. Schaake, R.H. Colby, Isothermal crystallization of poly(ether ether ketone) with different molecular weights over a wide temperature range, Polym. Cryst. 2 (2019) e10055, https://doi.org/10.1002/pcr2.10055.
- [2] M. Yuan, J.A. Galloway, R.J. Hoffman, S. Bhatt, Influence of molecular weight on rheological, thermal, and mechanical properties of PEEK, Polym. Eng. Sci. 51 (2011) 94–102, https://doi.org/10.1002/pen.21785.
- [3] J. Hu, H. Zhang, S. Li, C. Ji, S. Chen, Z. Zhou, B. Wang, Process parameter–mechanical property relationships and influence mechanism of advanced CFF/PEEK thermoplastic composites, Polym. Compos. 43 (2022) 5119–5132, https://doi.org/10.1002/pc.26801.
- [4] M.F. Talbott, G.S. Springer, L.A. Berglund, The Effects of Crystallinity on the Mechanical Properties of PEEK Polymer and Graphite Fiber Reinforced PEEK, J. Compos. Mater. 21 (1987) 1056–1081, https://doi.org/10.1177/ 002199838702101104
- [5] S. Ding, B. Zou, P. Wang, H. Ding, Effects of nozzle temperature and building orientation on mechanical properties and microstructure of PEEK and PEI printed by 3D-FDM, Polym. Test. 78 (2019), 105948, https://doi.org/10.1016/j. polymertesting.2019.105948.
- [6] P. Cebe, S.-D. Hong, Crystallization behaviour of poly(ether-ether-ketone), Polymer (Guildf) 27 (1986) 1183–1192, https://doi.org/10.1016/0032-3861(86) 00006-6
- [7] J.Y. Chen, M. Chen, S.C. Chao, Thermal stability and crystallization kinetics of poly (ether ether ketone), Macromol. Chem. Phys. 199 (1998) 1623–1629, https://doi. org/10.1002/(SICI)1521-3935(19980801)199:8<1623::AID-MACP1623>3.0.CO; 2.9623
- [8] M. Day, Y. Deslandes, J. Roovers, T. Suprunchuk, Effect of molecular weight on the crystallization behaviour of poly(aryl ether ether ketone): a differential scanning calorimetry study, Polymer (Guildf) 32 (1991) 1258–1266, https://doi.org/ 10.1016/0032-3861(91)90230-G.
- [9] J. Seo, X. Zhang, R.P. Schaake, A.M. Rhoades, R.H. Colby, Dual Nakamura model for primary and secondary crystallization applied to nonisothermal crystallization of poly(ether ether ketone), Polym. Eng. Sci. 61 (2021) 2416–2426, https://doi. org/10.1002/pep.25767
- [10] D.J. Blundell, B.N. Osborn, The morphology of poly(aryl-ether-ether-ketone), Polymer (Guildf) 24 (1983) 953–958, https://doi.org/10.1016/0032-3861(83) 00144.1
- [11] X. Zhang, A. Gohn, G. Mendis, J.F. Buzinkai, S.J. Weigand, A.M. Rhoades, Probing three distinct crystal polymorphs of melt-crystallized polyamide 6 by an integrated fast scanning calorimetry chip system, Macromolecules 54 (2021) 7512–7528, https://doi.org/10.1021/acs.macromol.1c00811.
- [12] Y. Furushima, A. Toda, V. Rousseaux, C. Bailly, E. Zhuravlev, C. Schick, Quantitative understanding of two distinct melting kinetics of an isothermally crystallized poly(ether ether ketone), Polymer (Guildf) 99 (2016) 97–104, https://doi.org/10.1016/j.nolymer.2016.07.005.
- [13] V. Mathot, M. Pyda, T. Pijpers, G. vanden Poel, E. van de Kerkhof, S. van Herwaarden, F. van Herwaarden, A. Leenaers, The Flash DSC 1, a power compensation twin-type, chip-based fast scanning calorimeter (FSC): first findings on polymers, Thermochim. Acta 522 (2011) 36–45, https://doi.org/10.1016/j. tca.2011.02.031.
- [14] E. Zhuravlev, C. Schick, Fast scanning power compensated differential scanning nano-calorimeter: 1. The device, Thermochim. Acta 505 (2010) 1–13, https://doi. org/10.1016/j.tca.2010.03.019.
- [15] E. Zhuravlev, C. Schick, Fast scanning power compensated differential scanning nano-calorimeter: 2. Heat capacity analysis, Thermochim. Acta 505 (2010) 14–21, https://doi.org/10.1016/j.tca.2010.03.020.

- [16] A. Toda, R. Androsch, C. Schick, Insights into polymer crystallization and melting from fast scanning chip calorimetry, Polymer (Guildf) 91 (2016) 239–263, https:// doi.org/10.1016/j.polymer.2016.03.038.
- [17] X. Zhang, J. Buzinkai, E. Quinn, A. Rhoades, Key insights into the differences between bimodal crystallization kinetics of polyamide 66 and polyamide 6, Macromolecules 55 (2022) 9220–9231, https://doi.org/10.1021/acs. macromol.2c01059.
- [18] Y. Lee, R.S. Porter, Crystallization of poly(etheretherketone) (PEEK) in carbon fiber composites, Polym. Eng. Sci. 26 (1986) 633–639, https://doi.org/10.1002/ pen.760260909.
- [19] P. Wang, Q. Lin, Y. Wang, C. Liu, C. Shen, Comparative study of the crystallization behavior and morphologies of carbon and glass fiber reinforced poly(ether ether ketone) composites, Polym. Polym. Compos. 29 (2021) 1229–1239, https://doi. org/10.1177/0967391120965102.
- [20] X. Yang, Y. Wu, K. Wei, W. Fang, H. Sun, Non-isothermal crystallization kinetics of short glass fiber reinforced poly (ether ether ketone) composites, Materials 11 (2018) 2094, https://doi.org/10.3390/ma11112094.
- [21] H. Sun, X. Yang, K. Wei, Y. Wu, W. Fang, Non-isothermal crystallization kinetics of continuous glass fiber-reinforced poly(ether ether ketone) composites, J. Therm. Anal. Calorim. 138 (2019) 369–378, https://doi.org/10.1007/s10973-019-08245-
- [22] E.J.H. Chen, B.S. Hsiao, The effects of transcrystalline interphase in advanced polymer composites, Polym. Eng. Sci. 32 (1992) 280–286, https://doi.org/ 10.1002/pen.760320408.
- [23] K. Naresh, K.A. Khan, R. Umer, W.J. Cantwell, The use of X-ray computed tomography for design and process modeling of aerospace composites: a review, Mater. Des. 190 (2020), 108553, https://doi.org/10.1016/j.matdes.2020.108553.
- [24] G. Vanden Poel, D. Istrate, A. Magon, V. Mathot, Performance and calibration of the Flash DSC 1, a new, MEMS-based fast scanning calorimeter, J. Therm. Anal. Calorim. 110 (2012) 1533–1546, https://doi.org/10.1007/s10973-012-2722-7.
- [25] P. Patel, T.R. Hull, R.W. McCabe, D. Flath, J. Grasmeder, M. Percy, Mechanism of thermal decomposition of poly(ether ether ketone) (PEEK) from a review of decomposition studies, Polym. Degrad. Stab. 95 (2010) 709–718, https://doi.org/ 10.1016/j.polymdegradstab.2010.01.024.
- [26] T. Ogasawara, T. Tsuda, N. Takeda, Stress-strain behavior of multi-walled carbon nanotube/PEEK composites, Compos. Sci. Technol. 71 (2011) 73–78, https://doi. org/10.1016/j.compscitech.2010.10.001.
- [27] T. Deák, T. Czigány, Chemical composition and mechanical properties of basalt and glass fibers: a comparison, Text. Res. J. 79 (2009) 645–651, https://doi.org/ 10.1177/0040517508095597.
- [28] M. Avrami, Kinetics of phase change. I: general theory, J. Chem. Phys. 7 (1939) 1103–1112, https://doi.org/10.1063/1.1750380.
- [29] M. Avrami, Kinetics of phase change. II Transformation-time relations for random distribution of nuclei, J. Chem. Phys. 8 (1940) 212–224, https://doi.org/10.1063/ 1.1750631.
- [30] E. Zhuravlev, A. Wurm, P. Pötschke, R. Androsch, J.W.P. Schmelzer, C. Schick, Kinetics of nucleation and crystallization of poly(e-caprolactone) - Multiwalled carbon nanotube composites, Eur. Polym. J. 52 (2014), https://doi.org/10.1016/j.eurpolymj.2013.12.015.
- [31] A. Wurm, A. Herrmann, M. Cornelius, E. Zhuravlev, D. Pospiech, R. Nicula, C. Schick, Temperature dependency of nucleation efficiency of carbon nanotubes in PET and PBT, Macromol. Mater. Eng. 300 (2015) 637–649, https://doi.org/ 10.1002/mame.201400405.
- [32] Y. Furushima, S. Kumazawa, H. Umetsu, A. Toda, E. Zhuravlev, A. Wurm, C. Schick, Crystallization kinetics of poly(butylene terephthalate) and its talc composites, J. Appl. Polym. Sci. 134 (2017) 44739, https://doi.org/10.1002/ app.44739.
- [33] X. Tardif, B. Pignon, N. Boyard, J.W.P. Schmelzer, V. Sobotka, D. Delaunay, C. Schick, Experimental study of crystallization of PolyEtherEtherKetone (PEEK) over a large temperature range using a nano-calorimeter, Polym. Test. 36 (2014) 10–19, https://doi.org/10.1016/j.polymertesting.2014.03.013.
- 10–19, https://doi.org/10.1016/j.polymertesting.2014.03.013.
   [34] A.A. Stepashkin, D.I. Chukov, F.S. Senatov, A.I. Salimon, A.M. Korsunsky, S. D. Kaloshkin, 3D-printed PEEK-carbon fiber (CF) composites: structure and thermal properties, Compos. Sci. Technol. 164 (2018) 319–326, https://doi.org/10.1016/j.compscitech.2018.05.032.
- [35] E. Piorkowska, A. Galeski, J.-M. Haudin, Critical assessment of overall crystallization kinetics theories and predictions, Prog. Polym. Sci. 31 (2006) 549–575, https://doi.org/10.1016/j.progpolymsci.2006.05.001.